MANSOURA JOURNAL OF CHEMISTRY
Official Journal of Faculty of Science, Mansoura University, Egypt
E-mail: scimag@mans.edu.eg ISSN: 2974-4938

Multifunctional Mercury and Uranyl Complexes of Thiosemicarbazone Ligand for Bioinorganic Innovation

Menna-Allah Asaad[1], Gaber M. Abu El-Reash[1,*], Samira M. Abozeid[1,2], Mohammed M. El-Gamil[1,3]

[1]Department of Chemistry, Faculty of Science, Mansoura University, El-Gomhoria Street, 35516 Mansoura, Egypt

[2]Chemistry Department, Faculty of Science, New Mansoura University, New Mansoura City, Egypt

[3]Department of Toxic and Narcotic Drug, Forensic Medicine, Mansoura Laboratory, Medico legal Organization, Ministry of Justice, Mansoura, Egypt

**** Correspondence to:** gaelreash@mans.edu.eg, 01000373155*

Received:1/9/2025 Accepted:20/9/2025

Abstract: This study reports the synthesis and comprehensive characterization of novel metal complexes formed by coordinating a custom-designed thiosemicarbazone ligand with mercury(II) and uranium(VI) oxide ions. Structural and electronic properties were elucidated using elemental analysis, FT-IR, UV-Vis, ^{1}H NMR spectroscopy, and density functional theory (DFT) calculations. Spectroscopic data revealed that the ligand acts as an NS-bidentate donor in the Hg(II) complex and as an NNS-tridentate donor in the U(VI)O_2 complex. UV-Vis analysis confirmed ligand-to-metal charge transfer (LMCT) transitions, supporting the proposed geometries, while DFT-based molecular orbital analysis provided insights into electronic distribution and chemical reactivity. Geometry optimization suggested a tetrahedral arrangement around the Hg(II) center. Biological evaluation was conducted using the disk diffusion method for antimicrobial activity and the DPPH radical scavenging assay for antioxidant potential. Biological screening demonstrated moderate antimicrobial activity, particularly against Staphylococcus aureus and Bacillus cereus, alongside notable antioxidant potential, with an IC_{50} value of 0.047 mg/mL. These findings highlight the dual bioactivity and structural integrity of the synthesized complexes, suggesting their potential for future applications in therapeutics, sensing technologies, and catalysis.

keywords: Thiosemicarbazone, DFT, and antioxidant activity

Introduction

Schiff base ligands, particularly thiosemicarbazones (TSCs), have garnered considerable attention due to their diverse and potent biological activities, making them promising candidates for medical and environmental applications. Derived from the condensation of aldehydes or ketones with thiosemicarbazide derivatives, these compounds exhibit versatile coordination behavior commonly forming bidentate, tridentate, or tetradentate complexes with transition metals [1-3].Among them, substituted thiosemicarbazones stand out as robust chelating agents, offering multiple donor sites that facilitate complexation with a wide range of metal ions [4].

What distinguishes this study is its focus on the selective interaction of TSCs with toxic heavy metals such as mercury Hg(II) and radioactive uranyl ions UO_2^{2+}, both of which pose significant environmental and health hazards [5]. Unlike conventional ligands, the dual donor nature of the thioketone and azomethine groups in TSCs enables enhanced binding affinity and specificity, particularly toward soft and borderline metal ions. This dual functionality not only improves complex stability but also enhances spectrophotometric sensitivity; an advantage for detection and quantification.

Moreover, while previous research has largely concentrated on hard donor atoms (e.g.,

oxygen and nitrogen) for uranyl ion coordination, this work explores the underutilized potential of soft sulfur donor ligands, offering a novel pathway for complex formation. By investigating the unique electronic and structural properties of these ligands, this study aims to develop more efficient and selective systems for metal ion sensing and remediation, addressing critical gaps in current detection technologies.

Materials and methods

Reagents.

All chemicals and reagents utilized in this study, along with metal salts, were sourced from suppliers including BDH, Merck, and Sigma-Aldrich, and were employed as received without any further processing.

Characterization

The Perkin-Elmer 2400 analyzer played a vital role in overseeing the results of elemental analyses, with a particular emphasis on (C), (H), (N) and (S). To determine the concentrations of Hg(II), U(VI)O_2, and Cl^- ions, we utilized both volumetric and gravimetric techniques [6].For FT-IR spectroscopy, we employed a Mattson 5000 FT-IR spectrophotometer. Furthermore, we captured DMF-based UV-Vis spectra at ambient temperature using a Unicam UV2 spectrophotometer. The ^{1}HNMR spectrum of the complexes was recorded with a JEOL 400 MHz spectrometer in DMSO-d_6.

Ligand Synthesis.

The ligand prepared according to the procedure outlined in the literature [7]

Synthesis of Metal Complexes.

The synthesis of complexes involving Hg(II) and U(VI)O_2 was conducted using 1 mmol of $HgCl_2$ and $UO_2(CH_3CO_2)_2(H_2O)$ metal salts, which were refluxed with 1 mmol of ligand in an ethanolic solution for a duration of four hours.

The progress of the reaction was monitored using thin-layer chromatography (TLC). Upon completion, a green solid was obtained for the Hg(II) complex, while a brown solid was produced for the U(VI)O_2 complex. These products were subsequently filtered, rinsed with hot ethanolic solution, and dried using a CaCl2 desiccator. vacuum desiccator.

Molecular modeling

The cluster calculations were carried out using the DMol^3 module [8], which is part of the Materials Studio program specifically designed for large-scale density functional theory (DFT) calculations. For the DSPP calculations, which involve DFT semi-core pseudopotentials, we utilized DNP (double numerical basis sets plus polarization functional) [9]. The quality of the DNP basis sets is on par with the 6-31G Gaussian basis sets. Research has demonstrated that DNP basis sets offer greater accuracy compared to Gaussian basis sets of the same size. Currently, the RPBE functional stands out as the best exchange-correlation functional, based on the generalized gradient approximation (GGA), and it effectively accounts for the exchange and correlation effects of electrons. Geometric optimization is performed without any symmetry constraints [10].

Biological applications

Antimicrobial activity

The study investigates the antimicrobial properties of the ligand H_2L and its complex with Hg(II) using the agar diffusion method [11, 12]. The evaluation involved testing against both Gram-negative bacteria, specifically *Escherichia coli* and *Entero bactercolacae* Gram-positive bacteria, including *Staphylococcus aureus* and *Bacillus cereus*.

DMSO was utilized as a negative control, while Gentamicin was employed as a standard antibiotic for comparison. The antibacterial activity was quantified by measuring the diameter of the inhibition zones created by the test compounds.

The % activity index was calculated by the formula as under:

$$\% \text{ Activity Index} = \frac{\text{Zone of inhibition by test compound(diametre)}}{\text{Zone of inhibition by standard (diametre)}} X100$$

Antioxidant activity using DPPH assay:

The antioxidant potential of the compounds under investigation was evaluated using the DPPH• colorimetric method, with standard ascorbic acid serving as a reference, as documented [13]. The electron donor capability

of the compounds was employed to quantify the reduction of a stable DPPH-free radical, transitioning from purple to yellow diphenyl picryl hydrazine. Stock solutions were prepared by dissolving samples in DMSO at a concentration of 7 mg/ml, and each sample was recorded at 517 nm.

Results and Discussion

Table 1 presents a summary of the molecular formulas, elemental analysis, and various physical characteristics of the Hg(II), and $U(VI)O_2$ complexes. The values of molar conductivity of Hg(II) complex was 32 ohm^{-1} cm^2 mol^{-1} indicating its electrolytic nature [14]

Table 1: Analytical and physical data of ligand and metal complexes

Compound molecular formula	(F.wt)	color	M.P. (^oC)	Found (calcd.)%						yield %	molar conductivity ohm^{-1} cm^2 mol^{-1}
				M	Cl	C	H	N	S		
$[Hg(HL)_2].Cl.H_2O.$ $C_{20}H_{27}ClHgN_{10}O_3S_2$	755.67	Green	>300	(26.54) (26.56)	4.53 (4.69)	(31.58) (31.78)	(3.58) (3.60)	(18.43) (18.54)	(8.34) (8.49)	70	32
$[UO_2(HL)(H_2O)(OAC)]$ $C_{12}H_{17}UN_5O_6S$	597.39	Brown	>300	(39.75) (39.85)	--- ---	(24.00) (24.13)	(2.67) (2.87)	(11.56) (11.72)	(5.23) (5.37)	65	---

FT-IR Spectroscopy (Table 2)

In the IR spectrum of the Hg^{2+} complex (1) shown in Figure 1, the spectrum reveals a distinct band at 3173 cm^{-1}, which corresponds to the ν(NH) vibration. Additionally, there's a band at 3213 cm^{-1} attributed to the $\nu(H_2O)$ mode, while the band at 1643 cm^{-1} relates to azomethine. The observe a new azomethine band at 1578 cm^{-1}, and the band at 1523 cm^{-1} refers to the $\nu(C=N)_{ox}$ band. Other notable bands include thioamide vibrations at 1464, 1335, 1142, and 855 cm^{-1}, along with ν(C=S) at 769 cm^{-1} and ν(N-N) vibrations at 1006 cm^{-1}. Bands at 1603, and 613 cm^{-1} refers to the $\nu(C=N)_{py}$ and $\delta(C=N)_{py}$ band confirms that Hg^{2+} exists in a monobasic NS bidentate. In the IR spectrum of the $(UO_2)^{2+}$ complex (2) shown in Figure 2, The spectrum shows a clear band at 3172 cm^{-1}, which is linked to the ν(NH) vibration. There's also a band at 3231 cm^{-1} that corresponds to the $\nu(H_2O)$ mode, and at 1641 cm^{-1} a band associated with azomethine. Additionally, a new azomethine band appears at 1583 cm^{-1}, while the band at 1528 cm^{-1} is related to the $\nu(C=N)_{ox}$ band. Other significant bands include thioamide vibrations at 1475, 1336, 1197, and 855 cm^{-1}, along with ν(C=S) at 769 cm^{-1} and ν(N-N) vibrations at 1006 cm^{-1} [15]. The shift of bands of $\nu(C=N)_{py}$ and $\delta(C=N)_{py}$ to 1617 and 641 cm^{-1} confirm the ligand behaves as a monobasic NNS tridentate in uranyl complex.

Table 2: IR bands of H_2L^1 and its metal complexes.

Compound		**H_2L**	**$[Hg(HL)_2].Cl.H_2O$**	**$[UO_2(HL)(H_2O)(OAC)]$**
$\nu(NH)^a$		3193	3173	3172
$\nu(NH)^b$		3103	-	-
$\nu(C=N)_{az}$		1633	1643	1641
$\nu(C=N)_{py}$		1604	1603	1617
$\delta(C=N)_{py}$		615	613	641
ν(N-N)		1011	1006	1009
Thioamide	(I)	1464	1441	1475
	(II)	1335	1336	1336
	(III)	1142	1181	1197
	(IV)	770	767	769
$\nu(C=N)^*$		-	1578	1583
$\nu(C=N)_{ox}$		1520	1523	1528

Electronic spectra :

The electronic spectral characteristics of the metal complexes in DMF reveal some interesting details. When we look at the spectrum of the diamagnetic Hg^{2+} complex, $[Hg(HL)_2].Cl.H_2O$, we can see a subtle shift in the energy of the bands, which is attributed to the $n\rightarrow\pi^*$ and $\pi\rightarrow\pi^*$ transitions. Moreover, the broad feature at 21881 cm^{-1} (457 nm) is associated with ligand-to-metal charge transfer (LMCT) [13]. This spectrum, combined with the observed diamagnetic behavior, supports

the structure depicted in Figure 2. Similarly, the spectrum of the diamagnetic U(VI)O_2 complex, [UO_2(HL)(H_2O)(OAC)], shows a slight change in the energy levels of the bands due to the n→π* and π → π* transitions. Additionally, the broad band at 23474 cm^{-1} (426 nm) is also linked to LMCT. Together, the spectrum and the diamagnetic behavior suggest a specific structure.

The ^{1}H NMR spectra

The ^{1}H NMR spectra for the Hg(II) and UO_2(II) metal complexes were recorded in a d_6-dimethylsulfoxide (DMSO-d_6) solution (figures 3 and 4). For the Hg(II) complex, we noticed the NH proton signals appearing at 10.308 ppm, 11.347 ppm, and 11.649 ppm. The protons at 1.24 ppm, 1.34 ppm, 1.98 ppm, and 2.03 ppm correspond to aliphatic protons, specifically four CH_3 protons. Meanwhile, the signals between 6.992 ppm and 8.538 ppm are typical of the aromatic ring. As for the UO_2(II) complex, we detected the NH proton signals at 11.136 ppm and 11.327 ppm. The protons at 2.490 ppm and 2.594 ppm are linked to aliphatic protons, specifically two CH_3 protons, while the signals from 7.124 ppm to 8.427 ppm are characteristic of the aromatic ring. Additionally, the signal at 15.876 ppm is associated with the OH group.

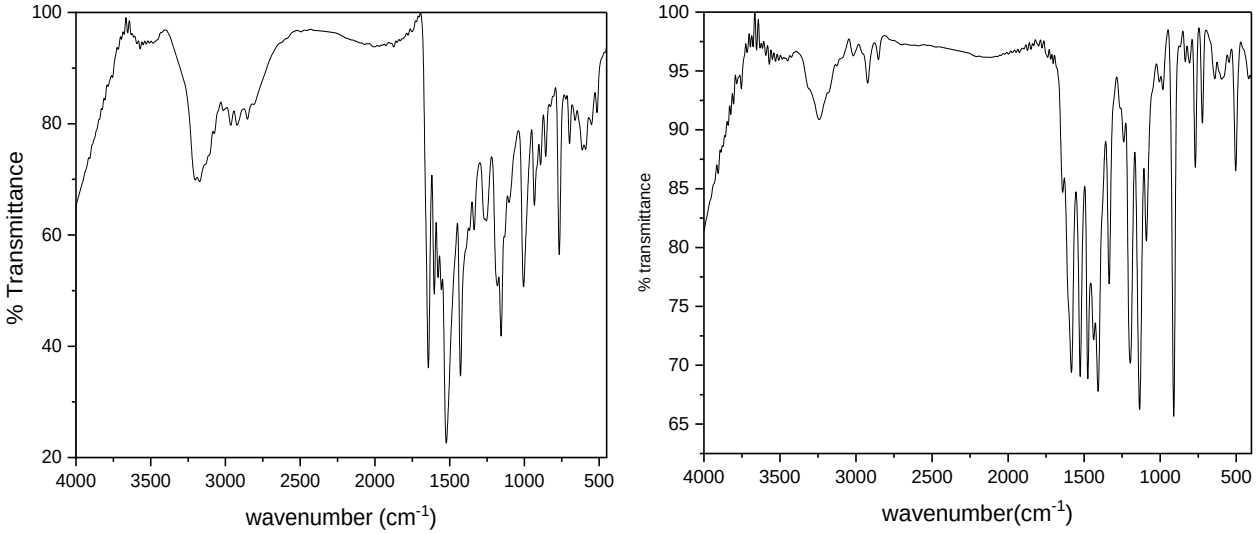

Hg(II)-complex **U(VI)O_2-complex**

Figure 1: FT-IR Spectra of Hg(II) and U(VI)O_2 Complexes

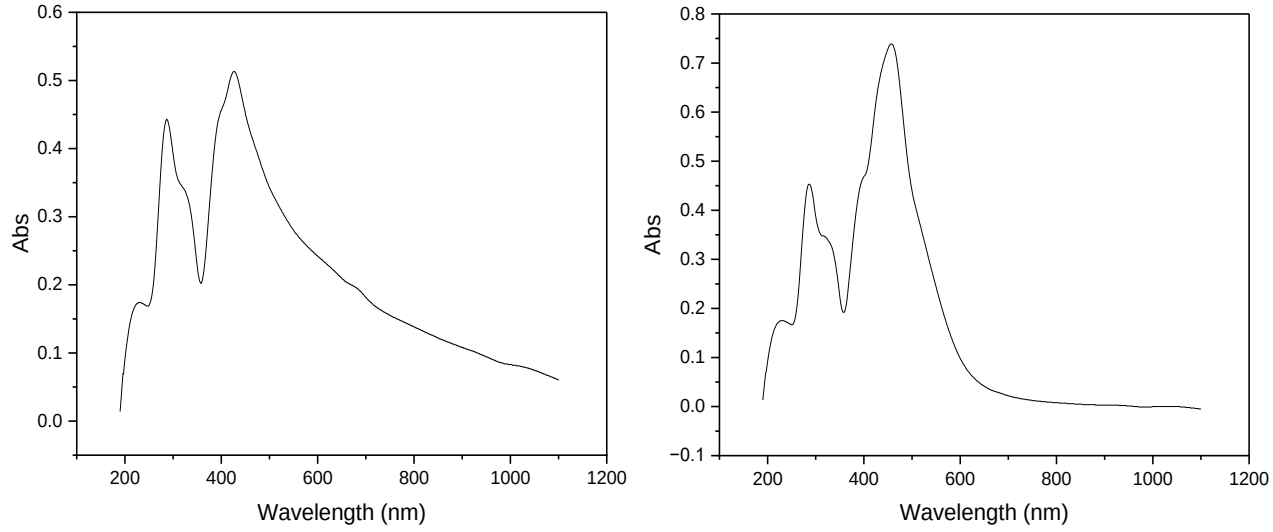

Hg(II)-complex **U(VI)O_2-complex**

Figure 2: UV-vis. Spectra in DMSO of Hg(II) and U(VI)O_2 complexes

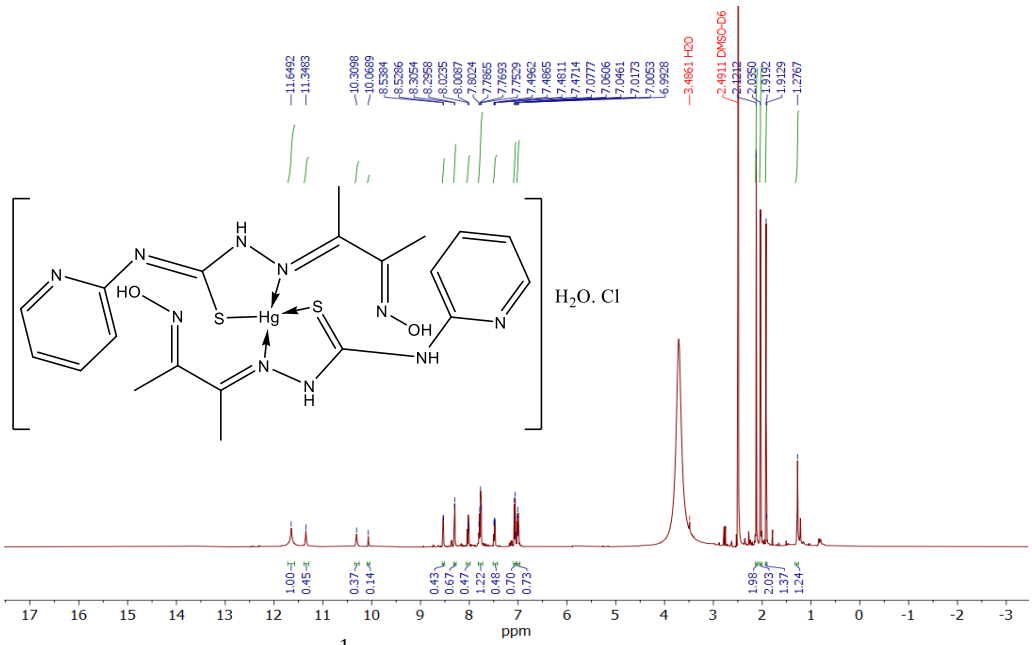

Figure 3: ^{1}HNMR Spectrum of Hg(II) complex.

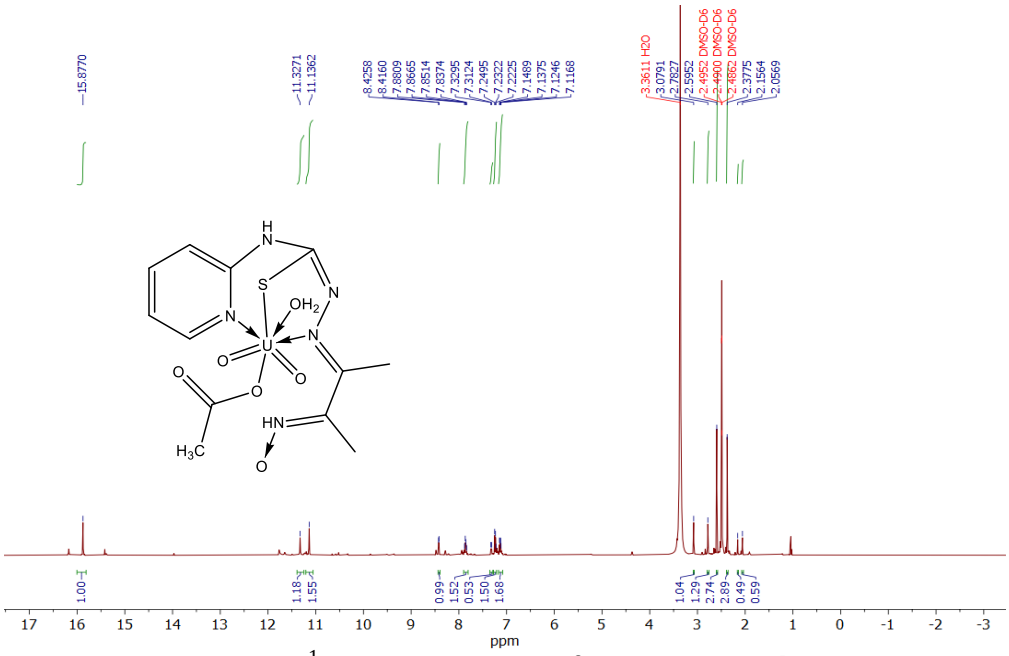

Figure 4: ^{1}HNMR Spectrum of U(VI)O_2 complex.

Molecular modeling

Geometry optimization

The optimized configurations and atomic numbers of the metal complex $[Hg(HL)_2].Cl.H_2O$ is illustrated in Figure 5 whereas the complex exhibited tetrahedral geometry. Additionally, the bond lengths and angles was recorded in tables 3 and 4.

Frontier Molecular Energies

Frontier molecular orbitals, namely the HOMO and LUMO, are crucial in assessing chemical reactivity. Molecules that possess smaller gaps between the HOMO and LUMO demonstrate increased reactivity and a heightened tendency for charge transfer, attributable to their reduced stability and increased softness [16].

Table 3: Selected bond lengths (Å) of $[Hg(HL)_2].Cl.H_2O$ using DFT method from DMOL^3 calculations

Bond	Length	Bond	Length
C(28)-N(26)	1.272	S(21)-Hg(35)	2.462
N(26)-C(25)	1.262	S(14)-Hg(35)	2.538
N(24)-H(49)	1.019	N(12)-Hg(35)	2.192
N(23)-Hg(35)	2.196	C(10)-S(14)	1.722
S(21)-H(61)	1.366		

Table 4: Selected bond angles (°) of $[Hg(HL)_2].Cl.H_2O$ using DFT-method from DMOL[3] calculations

Bond	Angle	Bond	Angle
N(23)-Hg(35)-S(21)	97.923	H(61)-S(21)-Hg(35)	34.021
N(23)-Hg(35)-S(14)	113.593	H(61)-S(21)-C(25)	96.526
N(23)-Hg(35)-N(12)	113.536	Hg(35)-S(21)-C(25)	109.931
S(21)-Hg(35)-S(14)	113.667	Hg(35)-S(14)-C(10)	70.441
S(21)-Hg(35)-N(12)	113.661	Hg(35)-N(12)-C(13)	122.731
N(24)-N(23)-C(22)	118.978	Hg(35)-N(12)-N(11)	75.509
S(14)-Hg(35)-N(12)	104.805	S(21)-Hg(34)-N(12)	114.287

Global chemical reactivity descriptions

The energy gap plays a crucial role in calculating various chemical descriptors, including electronegativity (χ), electrophilicity (ω), softness (S), chemical potential (μ), and hardness (η), which are summarized in Table 5. The calculations are as follows:

$\chi = -1/2\ (E_{LUMO} + E_{HOMO})$,

$\mu = -\chi = 1/2\ (E_{LUMO} + E_{HOMO})$,

$\eta = 1/2\ (E_{LUMO} - E_{HOMO})$,

$S = 1/2\ \eta$,

$\omega = \mu^2 / 2\eta$.

Table 5. Computed E_{HOMO}, E_{LUMO}, energy band gap ($E_H - E_L$), chemical potential (μ), electronegativity (χ), global hardness (η), global softness (S), and global electrophilicity index (ω) for $[Hg(HL)_2].Cl.H_2O$ complex

Compound	E_H(eV)	E_L(eV)	E_H-E_L(eV)	μ(eV)	χ (eV)	η(eV)	S(eV^{-1})	ω(eV)
$[Hg(HL)_2].Cl.H_2O$	-3.669	-3.440	0.259	-3.569	3.569	0.130	0.0647	49.19433

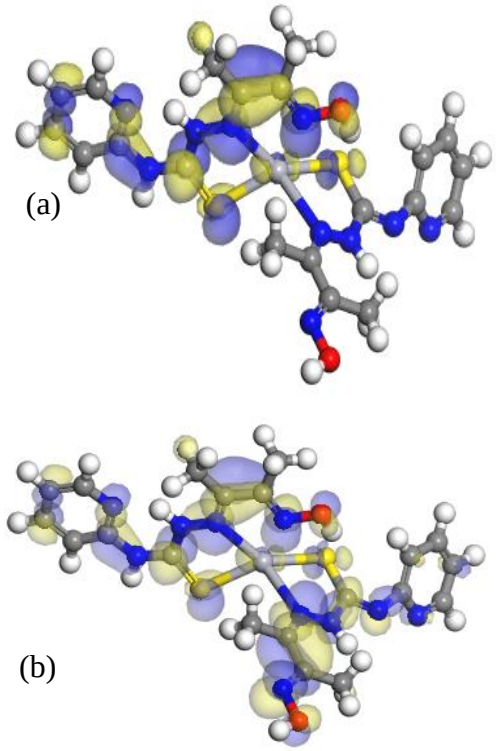

Figure 5: (a) HOMO and (b) LUMO orbitals of Hg(II)-complex

Molecular Electrostatic Potential Maps (MESP)

The Molecular Electrostatic Potential (MESP) is a 3D representation of the energy potential generated by a molecule's electron distribution (figure 6). It provides insights into charge distribution and aids in predicting chemical reactivity. By analyzing a molecule's electrostatics, one can understand its interactions with the surrounding environment. MESP is particularly valuable in the study of biomolecules, such as DNA and proteins, and plays a crucial role in drug and material design [17].

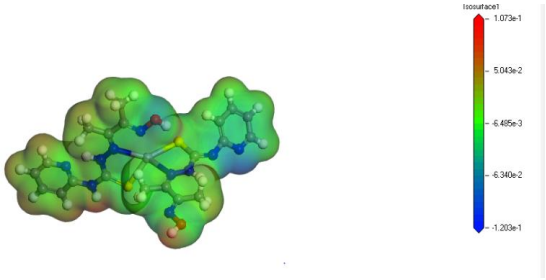

Figure 6: Colored MESP Map of Hg(II) complex

Biological studies

Anti-microbial activities

The novel complexes being investigated were assessed utilizing the aforementioned method [13] for in vitro anti-microbial evaluation against various bacterial species as

in the **table 6**. The table presents inhibition zone diameters (mm) for $[Hg(HL)_2].Cl.H_2O$ and gentamicin against both Gram-negative (G−) and Gram-positive (G+) bacterial strains, providing insights into the compound's spectrum of activity.

$[Hg(HL)_2].Cl.H_2O$ complex exhibits moderate antibacterial activity against *E. coli* (12 mm), *Staphylococcus aureus* (15 mm), and *Bacillus cereus* (12 mm). Furthermore, it shows weaker activity against Enterobacter cloacae (8 mm), a G− strain possibly more resistant due to outer membrane permeability.

Polar solvent, DMSO has no activity on microbial organisms but it was used to enhance solubility of polar ligands and metal complexes, improving their interaction with biological targets.

In general, the activity could be related to rich organic moiety with donor atoms, the strength of the metal-ligand bond, besides other factors such as size of the cation, receptor sites, diffusion and a combined effect of the metal and ligand for inactivation of the biomolecules [18]

Table 6: The evaluation of bacterial sensitivity (mm) shown by the **$[Hg(HL)_2]H_2O.Cl$** complex in relation to a variety of bacterial strains.

Compound	Inhibition zones diameters (mm/mg sample)			
	G- bacteria		G+ bacteria	
	E. coli	Enterobacter colacae	Staphylococcus aureus	Bacillus cereus
$[Hg(HL)_2].Cl.H_2O$	12	8	15	12
Control (DMSO)	-	-	-	-
Gentamicin	15	14	17	20

DPPH Antioxidant Activity

Table 7 compares the IC_{50} values (mg/ml) of ascorbic acid and the synthesized Hg(II) complex, reflecting their ability to scavenge free radicals.

The IC_{50} value of **Hg(II) Complex** (IC_{50} = 0.0470 mg/ml) exhibits moderate antioxidant activity. Although less effective than ascorbic acid, the value still indicates biologically relevant free radical inhibition.

Table 7. IC_{50} values of DPPH for the $[Hg(HL)_2].Cl.H_2O$ complex.

Compounds	Ascorbic acid	Hg(II) complex
IC_{50} (mg/ml)	0.0222	0.0470

4. Conclusion

In this investigation, novel complexes of Hg(II) and $U(VI)O_2$ were synthesized through targeted coordination with a custom ligand, leading to well-defined products exhibiting robust structural features. Spectroscopic analyses, including FT-IR, UV-Vis, and ^1H NMR, affirmed distinct coordination behaviors, where the Hg(II) complex adopts an NS-bidentate binding mode and the $U(VI)O_2$ complex functions via an NNS-tridentate arrangement. These coordination environments were further validated by density functional theory (DFT) calculations, which provided optimized geometries, frontier orbital

parameters, and molecular electrostatic potential maps that reveal charge distribution and reactive domains. Chemical reactivity descriptors, such as electrophilicity and softness, confirmed their moderate chemical responsiveness.

Biological assays demonstrated that the Hg(II) complex possesses antimicrobial efficacy against both Gram-positive and Gram-negative strains, with a stronger effect observed against *Staphylococcus aureus* and *Bacillus cereus*. Additionally, the DPPH-based antioxidant assay indicated reasonable radical-scavenging activity, further reinforcing the compound's multifunctional biological relevance. These integrated findings suggest that the synthesized complexes hold potential in fields such as medicinal chemistry, antimicrobial development, and fluorescence sensing. Future work may explore structure-activity relationships, cytotoxicity profiles, and extended biomolecular interactions to uncover broader applications and enhance the compound's utility in targeted drug or sensor design.

5. References

1. V. Singh, V.N.V. Palakkeezhillam, V. Manakkadan, P. Rasin, A.K. Valsan, V.S. Kumar, (2023) A. Sreekanth, Recent developments on the potential biological applications of transition metal complexes of thiosemicarbazone derivatives, Polyhedron, **245** 116658.
2. S. Priyarega, J. Haribabu, R. Karvembu, (2022) Development of thiosemicarbazone-based transition metal complexes as homogeneous catalysts for various organic transformations, Inorganica Chimica Acta, **532** 120742.
3. R. Nickisch, P. Conen, M.A.R. Meier, (2022) Polythiosemicarbazones by Condensation of Dithiosemicarbazides and Dialdehydes, Macromolecules, **55** 3267–3275.
4. L. Feng, W. Shi, J. Ma, Y. Chen, F. Kui, Y. Hui, Z. Xie, (2016) A novel thiosemicarbazone Schiff base derivative with aggregation-induced emission enhancement characteristics and its application in Hg2+ detection, Sensors and Actuators B: Chemical, **237** 563–569.
5. C.V. Florea, G.O. Buică, M.A. Pandele, A.M. Onaş, M.-E. Voicu, A. Hanganu, V. Tecuceanu, G.-G. Vasile, C. Devan, R. Stan, M.D. Raicopol, (2024) Dual-function sensing platform for Hg(II) based on a redox-active thiosemicarbazone receptor, *Journal of Electroanalytical Chemistry*, **961** 118251.
6. A.I. Vogel, G.H. Jeffery, Vogel's textbook of quantitative chemical analysis, (1989).
7. U. El-Ayaan, G.A. El-Reash, I.M. Kenawy, (2003) Synthesis, Spectroscopic, and Magnetic Properties of Some Transition Metal Complexes with 4-(2-Pyridyl)-1-(diacetylmonoxime)-3-thiosemicarbazide, Synthesis and Reactivity in Inorganic and Metal-Organic Chemistry, **33** 327–342.
8. W. Wang, Y. Deng, X. Chen, X. Wang, Z. Zhao, B. He, H. Wang, W. Li, P. Xu, Q. Yin, (2022) Density functional theory study of ZnnInn (n= 2–10) alloy clusters, *Journal of Molecular Structure*, **1247** 131345.
9. A.F. Al-Hossainy, M.S. Zoromba, O.A. El-Gammal, F.I. El-Dossoki, (2019) Density functional theory for investigation of optical and spectroscopic properties of zinc-quinonoid complexes as semiconductor materials, Structural Chemistry, **30** 1365–1380.
10. A.M. Younis, M.M. El-Gamil, T.H. Rakha, G.M. Abu El-Reash, (2021) Iron(III), copper(II), cadmium(II), and mercury(II) complexes of isatin carbohydrazone Schiff base ligand (H 3 L): Synthesis, characterization, X-ray diffraction, cyclic voltammetry, fluorescence, density functional theory, biological activity, and molecular docking studies, Applied Organometallic Chemistry,.
11. A. Bauer, W. Kirby, J.C. Sherris, M. Turck, (1966) Antibiotic susceptibility testing by a standardized single disk method, American journal of clinical pathology, **45** 493–496.
12. M.A. Mohammed, A. Fetoh, T.A. Ali, M.M. Youssef, G.M. Abu El-Reash, (2023) Fabrication of novel Fe (III), Co (II), Hg (II), and Pd (II) complexes based on water-soluble ligand (NaH2PH): structural characterization, cyclic voltammetric, powder X-ray diffraction, zeta potential, and biological studies, Applied Organometallic Chemistry, **37** e6910.
13. D.M. Belal, U.I. El-Ayaan, M.M. El-Gamil, A.M. Younis, G.M.A. El-Reash, (2023) Fluorescence, cyclic voltammetric, computational, and spectroscopic studies of Mn(II), Co(II), Pd(II), Zn(II) and Cd(II) complexes of salen ligand and their biological applications, Journal of Molecular Structure, **1271** 134142.
14. P. Souza, F. Kaiser, J.R. Moguer, (1987) A. Arquero, Transition Met. Chem, **12** 128.
15. A. Singh, M. Bharty, R. Dani, S. Singh, S. Kushawaha, N. Singh, (2014) Manganese (II) and zinc (II) complexes of 4-phenyl (2-methoxybenzoyl)-3-thiosemicarbazide: Synthesis, spectral, structural characterization, thermal behavior and DFT study, Polyhedron, **73** 98–109.
16. N.T. Anh, (2007) Frontier orbitals: a practical manual, John Wiley & Sons,.

17. C.H. Suresh, G.S. Remya, P.K. Anjalikrishna, (2022) Molecular electrostatic potential analysis: A powerful tool to interpret and predict chemical reactivity, Wiley Interdisciplinary Reviews: Computational Molecular Science, **12** e1601.

18. R. Nagar, (1990) Syntheses, characterization, and microbial activity of some transition metal complexes involving potentially active O and N donor heterocyclic ligands, *J. Inorg. Biochem.*, **40** 349–356.